Temporal Filtering Enhances the Skewness of Sea Surface Winds

Adam H. Monahan

July 2018

Temporal Filtering Enhances the Skewness of Sea Surface Winds

ADAM H. MONAHAN

School of Earth and Ocean Sciences, University of Victoria, Victoria, British Columbia, Canada

(Manuscript received 30 November 2017, in final form 10 April 2018)

ABSTRACT

The component of the sea surface wind in the along-mean wind direction is known to display pronounced skewness at many locations over the ocean. A recent study by Proistosescu et al. found that the skewness of daily 850-hPa air temperature measured by radiosondes is typically reduced by bandpass filtering. This behavior was also shown to be characteristic of correlated additive–multiplicative (CAM) noise, which has been proposed as a generic model for non-Gaussian variability in the atmosphere and ocean. The present study shows that if the cutoff frequency is not too low, the skewness of the along-mean wind component is enhanced by low-pass filtering, particularly in the equatorial band and in the midlatitude storm tracks. The filter time scale beyond which skewness is systematically reduced by filtering is of the daily to synoptic scale, except in a narrow equatorial band where it is of subseasonal to seasonal time scales. This behavior is reproduced in an idealized stochastic model of the near-surface winds, in which key parameters are the characteristic time scales of the nonlinear dynamics and of the noise. These results point toward more general approaches for assessing the relative importance of multiplicative noise or dynamical nonlinearities in producing non-Gaussian structure in atmospheric and oceanic fields.

1. Introduction

Various atmospheric and oceanic fields are characterized by non-Gaussian variability, with distributions that are skewed, flatter (or more sharply peaked) than Gaussian, or multimodal. The presence of non-Gaussian variability in such fields has important implications for the distribution of extremes (Sardeshmukh et al. 2015) as well as for the distribution of quantities obtained from nonlinear functions of these fields such as surface fluxes or wind power densities. As discussed in the recent review by Sura and Hannachi (2015), a range of dynamic and kinematic mechanisms have been proposed to explain observed deviations from Gaussianity. The two mechanisms that have most commonly been proposed in modeling studies relate non-Gaussianity to dynamical nonlinearities or to multiplicative noise (itself reflecting nonlinear coupling between resolved state variables and unresolved variability parameterized as stochastic processes).

In general, the strength and character of non-Gaussian structure depend on how the data have been processed, such as by temporal or spatial filtering (e.g., Teng et al. 2004; Schneider et al. 2015). Proistosescu et al. (2016) considered the effects of bandpass filtering on the skewness and kurtosis of daily 850-hPa radiosonde temperatures. They showed that for these data, the skewness generally decreases as the bandpass width becomes narrower (although there are some small filter ranges where this behavior is not found). In particular, for fixed values of the low-frequency cutoff, the skewness generally decreases as the high-frequency cutoff is decreased.

This behavior was interpreted by Proistosescu et al. (2016) in terms of the bispectrum, which partitions the contributions of different frequencies to the third-order moment of the time series in a manner similar to that in which variance is partitioned by the power spectrum. They used a geometrical argument to demonstrate that the elimination of pairwise frequency interactions in the bispectrum by filtering results in the reduction of skewness of non-Gaussian white noise. In the absence of serial dependence, the value of the bispectrum is uniform across all pairs of frequencies in the same way that the spectrum of a white noise process is flat. As noted by Proistosescu et al. (2016), when the series under consideration is characterized by serial dependence, the elimination of frequency interactions by filtering will not necessarily have the same effect on the skewness. Proistosescu et al. (2016) therefore considered two examples of serially dependent stochastic processes [first-order autoregressive processes with

Corresponding author: Adam H. Monahan, monahana@uvic.ca

DOI: 10.1175/JCLI-D-17-0814.1

skewed Pearson-distributed noise and correlated additive–multiplicative (CAM) noise models; cf. Sardeshmukh and Sura 2009] and found qualitatively similar behavior to that found in the radiosonde data. Proistosescu et al. (2016) hypothesize that this behavior of the skewness under filtering is a consequence of the non-Gaussianity being introduced by processes on time scales short compared to the decorrelation time, and note that it may not generalize to all atmospheric quantities displaying non-Gaussian variability.

To investigate if the systematic skewness reduction by filtering is found in another markedly non-Gaussian atmospheric field, this study considers the effect of temporal filtering on the skewness of sea surface wind in the Modern-Era Retrospective Analysis for Research and Applications, version 2 (MERRA-2), reanalysis product. Specifically, the analysis considers the component of the 10-m wind vector parallel to the time-mean wind, which previous studies have shown is characterized by a pronounced skewness (Monahan 2004, 2006a). It is shown that for sufficiently high values of the cutoff frequency, the skewness of low-pass-filtered along-mean winds is enhanced by filtering, especially in a near-equatorial band and in the storm track regions (section 3). As the cutoff frequency becomes sufficiently low (corresponding to time scales beyond the synoptic scale in midlatitudes and the subseasonal scale in the equatorial band), the skewness is systematically reduced by filtering. This behavior is then interpreted in terms of an idealized stochastic model of the boundary layer momentum budget (section 4). Conclusions are presented in section 5.

2. Data

This analysis considers hourly 10-m zonal and meridional wind components from the MERRA-2 reanalysis product (Gelaro et al. 2017), on a 2° × 2.5° latitude–longitude grid between 60°S and 60°N from 1 January 1980 to 31 December 2016. These data were spatially subsampled (not averaged) from the original 0.5° × 0.625° grid to reduce calculation costs. This reanalysis product was selected because of its relatively high temporal resolution, which allows consideration of temporal scales of variability to extend to the Nyquist frequency of 12 cycles per day (cpd).

Previous studies have shown that the largest skewness values of sea surface winds are generally found in the component parallel to the mean wind (Monahan 2006a), so at each grid point the components are rotated from zonal and meridional to components along and across the mean wind vector. Because of the strong anticorrelation between the mean and skewness of the components, the skewness of the along-mean wind component is negative. To accommodate the fact that the orientation of the wind may vary seasonally, the mean vector is defined with a seasonal cycle that is computed using a harmonic fit to the zonal and meridional components (using the annual, semiannual, and terannual cycles). The resulting along- and across-wind components will be denoted respectively as u and v. The results of the following analysis are essentially unchanged if the time-mean vector wind without seasonal variations is used to define the along- and across-components. The effects of seasonality are further reduced by then subtracting the mean annual cycle defined above from u and dividing the resulting anomaly time series by a harmonic fit (including the annual and semiannual cycles) to the seasonal cycle of standard deviation. This approach to reducing the effects of seasonality was adopted, rather than conducting separate analyses in different calendar seasons, in order to allow for filtering periods longer than a season.

At each location, the along-mean wind component time series u is filtered using a two-point Butterworth bandpass filter with backward and forward passes (implemented using the MATLAB command filtfilt). The highest and lowest admitted frequencies of the filter will be respectively denoted f_U and f_L. To avoid endpoint effects at the beginning and end of the filtered time series, the first and last 10% of the time series are discarded before further statistical quantities are estimated. To assess the statistical significance of the estimated skewness values (against a null hypothesis that the distribution is Gaussian) the same approach as in Proistosescu et al. (2016) is used. The time series is Fourier transformed, random values, uniform on $[0, 2\pi)$, are assigned to the phases, and then the reverse transform is computed. The resulting time series has the same second-order statistics as the original (including the autocorrelation function) but has a distribution very close to Gaussian. Repeating this process for different random realizations of the phases allows estimation of the sampling distribution of the skewness for a Gaussian process with the same number of statistical degrees of freedom as the original time series. In the following analysis, statistical significance is assessed using random ensembles of 150 members. Filtered (negative) skewness values are considered significant if none of the filtered skewness values from the Gaussian ensemble exceeded the observed value.

3. Effects of filtering on observed along-mean sea surface wind component

The effect of bandpass filtering on the skewness of the along-mean wind component is shown for three

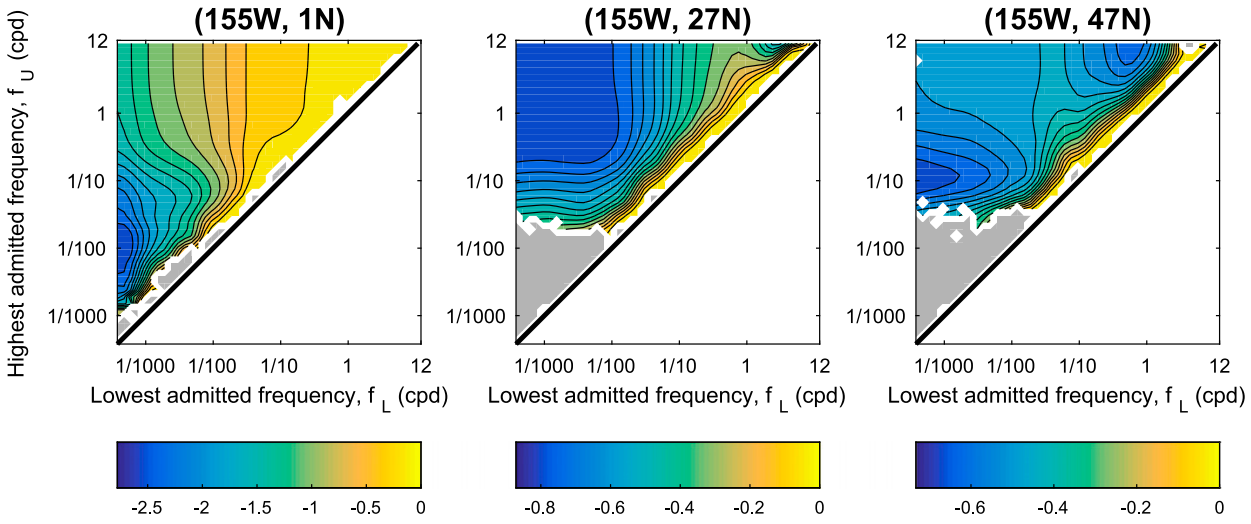

FIG. 1. Skewness of bandpass-filtered along-mean wind component at three representative locations, as functions of the upper and lower cutoff frequencies (respectively f_U and f_L), measured in cycles per day (cpd). The gray areas are regions where the skewness is not significantly different from zero at the 99% significance level. The significance test is described in the text.

representative locations in Fig. 1. In the individual panels of this figure, the horizontal and vertical axes are respectively the lowest and highest admitted frequencies, f_L and f_U. The upper-left corner corresponds to the unfiltered time series. Only those skewness values that are statistically significant at the 99% significance level are shown. At the first location (1°N, 155°W) in the equatorial east Pacific, the magnitude of the skewness of the bandpass-filtered time series for fixed f_U decreases monotonically as f_L becomes larger (so the filter band becomes narrower). In contrast, for fixed values of f_L, the magnitude of skew(u) initially increases as f_U decreases from the Nyquist frequency, taking a local extremum before decreasing toward zero as the bandpass window further narrows. For small values of f_L, the skewness of the filtered wind changes from a value of about −1.3 for the unfiltered time series to a local extremum of almost −2.5 at a high-pass cutoff frequency of about 1/100 cpd, beyond which it approaches zero as f_U is further decreased. At the second location (27°N, 155°W) in the subtropical North Pacific, the magnitude of skew(u) decreases monotonically as the width of the bandpass filter is narrowed. For fixed f_L, the skewness is initially unaffected for f_U decreasing away from the Nyquist frequency; beyond a threshold between 1 and 1/10 cpd, the skewness magnitude starts to decrease. No pronounced extremum is observed. Finally, behavior similar to that of the first location is observed at the third location (47°N, 155°W) in the midlatitude North Pacific, except that the local extremum occurs near 1/10 cpd. A second local extremum in f_L is also seen for narrow bandpass filtering with f_U between 1 and 12 cpd. The general reduction of skewness by bandpass filtering found in temperature observations by Proistosescu et al. (2016) is not a feature of this field.

The focus of the following analysis will be on the filtered along-mean sea surface wind skewness extremum for the smallest values of f_L, as this feature appears consistently at locations around the world (not shown). The analysis can then be simplified by considering the skewness of low-pass-filterd (rather than bandpass-filtered) along-mean wind as a function of the filter period $T = 1/f_c$ where f_c is the low-pass cutoff frequency. The low-pass-filtered time series u with cutoff period T will be denoted by $[u]_T$. Plots of skew($[u]_T$) as functions of T for the three locations previously considered (Fig. 2) clearly show the enhancement of skewness by filtering for the near-equatorial and midlatitude locations, with extrema respectively at $T \sim 100$ days and $T \sim 8$ days. The presence of a local extremum in skew($[u]_T$) at $T \sim 1$ day at the subtropical site is also evident, although this feature is weak. For T larger than this value at this location, low-pass filtering systematically reduces the magnitude of skew($[u]_T$).

The analysis of u is repeated for each location in the domain, computing the filter time scale $T_{\min}$ resulting in the largest absolute skewness, skew($[u]_{T_{\min}}$). The extremum is computed over the range of T values for which the skewness is significantly nonzero based on the test described in section 2. Maps of skew(u), skew($[u]_{T_{\min}}$), the difference between skew($[u]_{T_{\min}}$) and the unfiltered skew(u), and $T_{\min}$ (Fig. 3) all show clear geographical structure. Similar to the skewness

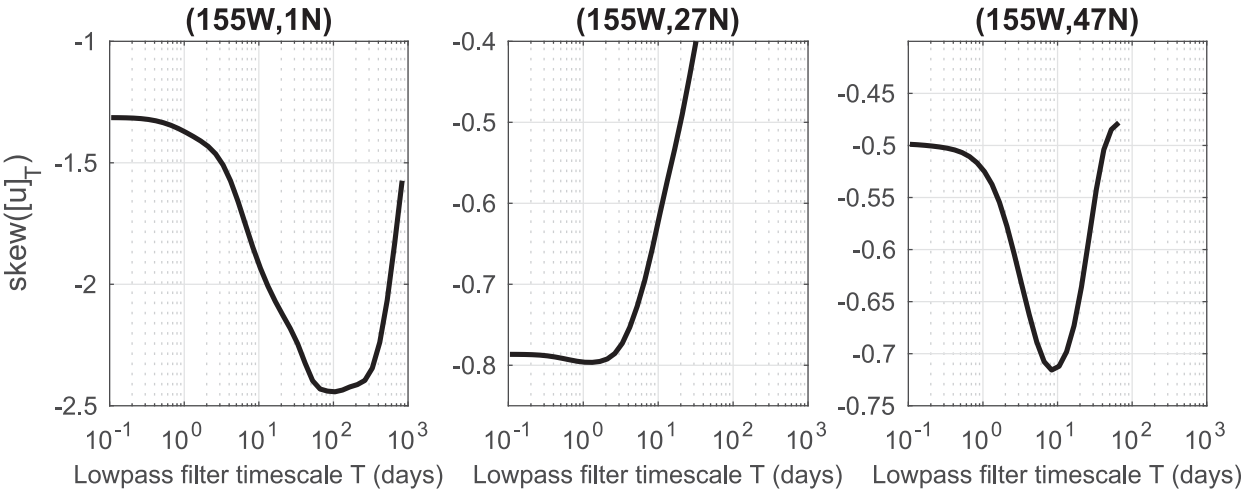

FIG. 2. Skewness of low-pass-filtered along-mean wind component $[u]_T$ as a function of the filter cutoff period $T = 1/f_c$, at the locations considered in Fig. 1. Skewness values that are not significant at the 99% significance level are not shown.

field of the unfiltered along-mean wind component, skew($[u]_{T_{\min}}$) takes large negative values in the storm tracks and the subtropics. The most negative filtered skewness values are found in a narrow equatorial band, particularly in the region centered around 150°W. In the zonal median, the skewness enhancement is near zero in the subtropics, on the order of −0.2 in the midlatitudes, and about −0.3 in the narrow equatorial belt. Locally, the skewness enhancement in the midlatitudes can be larger in magnitude than −0.5 and in the equatorial belt larger in magnitude than −1 (particularly near 150°W; cf. Fig. 2). Values of $T_{\min}$ range over orders of magnitude from a day or less in the subtropics to on the order of 7–10 days in the midlatitudes to 40–100 days in the equatorial belt. In most locations where the value of $T_{\min}$ is less than a day (particularly around 20°S), there is no skewness enhancement by filtering. In such locations, filtering has little effect on skew($[u]_T$) below a threshold of $T \sim$ 1–2 days, beyond which the magnitude is reduced as T increases.

Time series of u and $[u]_{T_{\min}}$ at the representative locations considered earlier are shown in Fig. 4. Also shown are kernel density estimates of the probability density functions (pdfs) of the standardized anomalies of u and $[u]_T$ (the time series divided by their respective standard deviations). At the equatorial location, the large value of $T_{\min}$ results in $[u]_{T_{\min}}$ having a variance 70% smaller than u. Large and sustained negative excursions associated with El Niño years are evident in both u and $[u]_{T_{\min}}$. At this location, the enhancement of skewness by filtering results from emphasizing these dominant seasonal and longer time scale anomalies while suppressing shorter than subseasonal fluctuations. The pdf of the filtered time series shows a much narrower core and a much more pronounced negative tail than the unfiltered time series. Time series of u and $[u]_{T_{\min}}$ at equatorial locations outside the eastern Pacific that also show strong skewness changes under filtering (not shown) do not show a pronounced El Niño signature. Time series of u and $[u]_{T_{\min}}$ at the subtropical location differ little, consistent with the relatively small value of $T_{\min}$ (such that the low-pass filter cuts out relatively little variance). No substantial difference exists between the pdfs of u and $[u]_{T_{\min}}$ at this location. Finally, the midlatitude location shows a filtered time series $[u]_{T_{\min}}$ that differs substantially from the raw series u (the variance is reduced by 56%), and the filtered pdf has an evidently greater tilt toward negative anomalies.

To summarize, three distinct regions are evident in the effect of low-pass filtering on the skewness of along-mean surface winds. In a narrow band around the equator, skewness values show a large enhancement when frequencies above the subseasonal-to-seasonal band are filtered out. In the midlatitudes (specifically the storm track regions) skewness shows a smaller but still substantial enhancement when synoptic and higher frequencies are removed. Finally, throughout the subtropics, only small enhancements of skewness are produced by filtering and reductions in the absolute skewness occur with the removal of frequencies on daily or longer time scales. In the subsequent section, an idealized model of the stochastic dynamics of surface winds is used to address the physical origin of these differences.

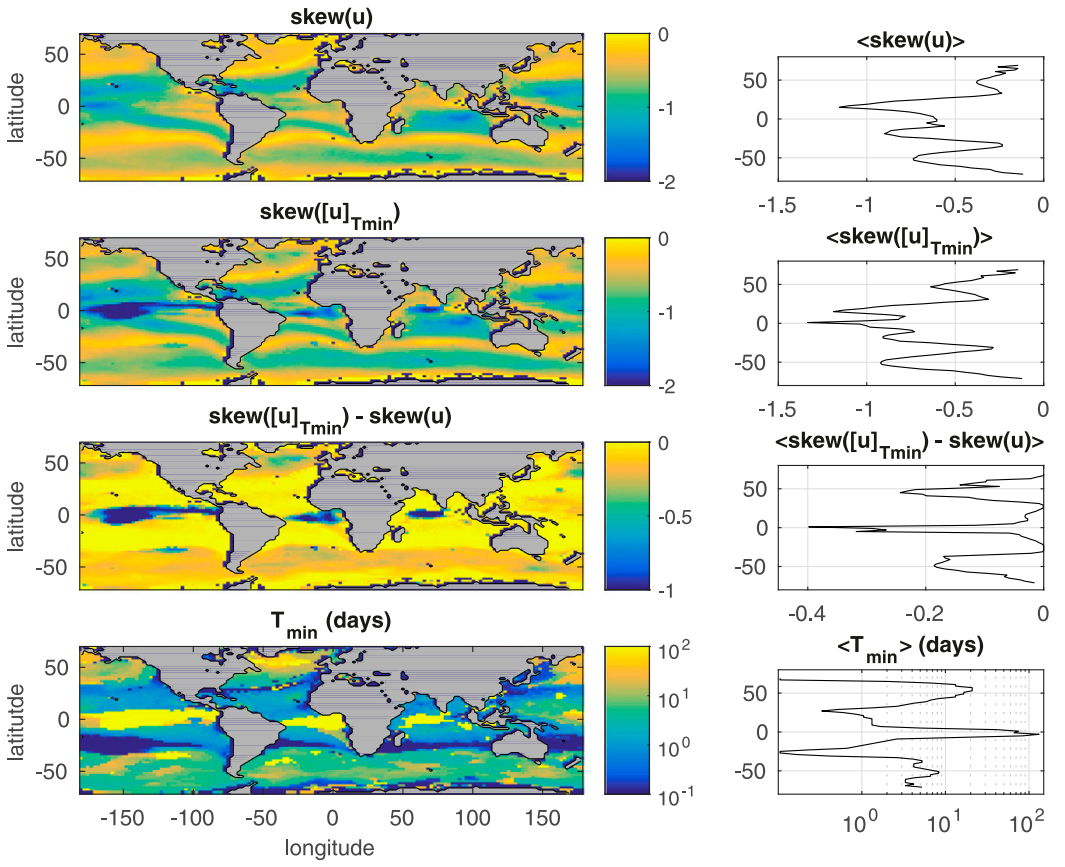

FIG. 3. (left) Maps of (top)–(bottom) the raw along-mean wind skewness, the largest filtered along-mean wind skewness $[u]_{T_{\min}}$, the difference between the largest filtered skewness and the unfiltered skewness values, and the filter time scale $T_{\min}$ at which the minimum skewness occurs. (right) Zonal medians of the quantities at (left).

4. Idealized surface wind model

The idealized surface wind model considered is a version of the stochastic surface momentum budget introduced in Monahan (2004, 2006a). Tendencies in the horizontal wind vector (u, v) averaged over a layer of thickness h are modeled as resulting from imbalances between the surface turbulent momentum flux (expressed using a bulk drag law with drag coefficient c_d, taken to be constant) and the ageostrophic difference between the pressure gradient and Coriolis forces:

$$\frac{d}{dt}u = \langle \Pi_u \rangle - \frac{c_d}{h}(u^2 + v^2)^{1/2}u + \eta_u \quad \text{and} \qquad (1)$$

$$\frac{d}{dt}v = -\frac{c_d}{h}(u^2 + v^2)^{1/2}v + \eta_v. \qquad (2)$$

The model assumes that tendencies associated with horizontal momentum advection are negligible and that the "large scale" ageostrophic residual between the pressure gradient and Coriolis forces can be expressed as the sum of a mean $(\langle \Pi_u \rangle, 0)$ and fluctuations (η_u, η_v), which are independent of u and v. Neglecting momentum exchange between this layer and the atmosphere above is equivalent to taking h to be the depth of the turbulent boundary layer, held constant for simplicity. By construction, there is no mean ageostrophic tendency in the budget of the crosswind component v.

Complete specification of the wind model requires modeling the fluctuating ageostrophic forcing (η_u, η_v). If these components are taken to be independent Gaussian white noise processes with the same intensity σ, then an analytic expression can be obtained for the stationary joint pdf of (u, v) (Monahan 2006a). However, the white noise approximation for these fluctuations has several limitations. In particular, the white noise model requires unrealistically large values of h to produce serial dependence similar to that observed, and it is unable to account for the strong anisotropy in the autocorrelation structure of the

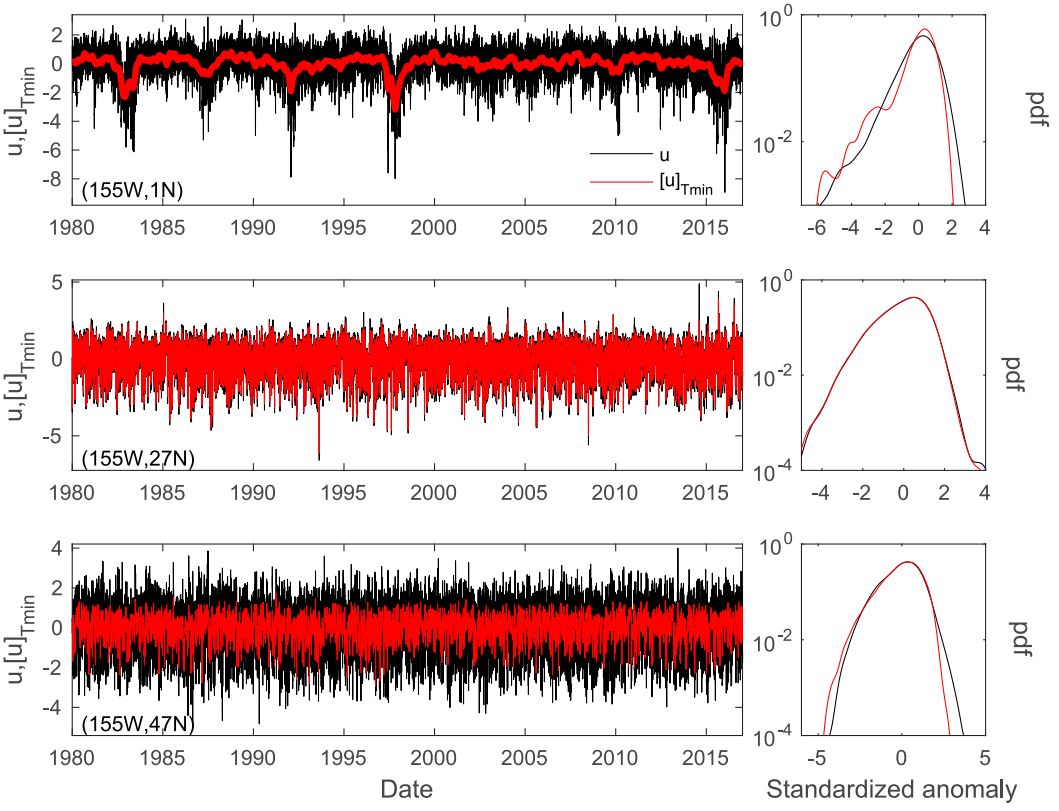

FIG. 4. (left) Time series of u (black) and $[u]_{T_{\min}}$ (red) at the representative locations from Figs. 1 and 2. (right) Kernel density estimates of the pdfs of the standardized anomalies of u and $[u]_{T_{\min}}$ (the time series less the mean and divided by the standard deviation).

wind components (Monahan 2012; Thompson et al. 2014). For this analysis, (η_u, η_v) will be modeled as independent Ornstein–Uhlenbeck ("red noise") processes:

$$\frac{d}{dt}\eta_u = -\frac{1}{\tau}\eta_u + \frac{\sigma}{\tau}\dot{W}_1 \quad \text{and} \tag{3}$$

$$\frac{d}{dt}\eta_v = -\frac{1}{\tau}\eta_v + \frac{\sigma}{\tau}\dot{W}_2, \tag{4}$$

where the $\dot{W}_j$ are independent Gaussian white noise processes with $E\{\dot{W}_i(t)\dot{W}_j(t')\} = \delta_{ij}\delta(t-t')$. For simplicity, the memory and scale parameters τ and σ for the two processes are taken to be the same. The scaling of the white noise processes is such that (η_u, η_v) approaches $(\sigma\dot{W}_1, \sigma\dot{W}_2)$ as $\tau \to 0$. One of the consequences of this modeling choice is that σ takes the unit $\mathrm{m\,s^{-3/2}}$ for wind components measured in $\mathrm{m\,s^{-1}}$.

Together, Eqs. (1)–(4) describe a four-dimensional stochastic differential equation with five parameters. The system can be simplified if it is nondimensionalized using the characteristic dynamical speed and time scales, respectively:

$$U = \left(\frac{\langle \Pi_u \rangle h}{c_d}\right)^{1/2} \quad \text{and} \tag{5}$$

$$\theta = \left(\frac{h}{\langle \Pi_u \rangle c_d}\right)^{1/2} = \frac{h}{U c_d}. \tag{6}$$

The resulting nondimensional model

$$\frac{d}{d\tilde{t}}\tilde{u} = 1 - (\tilde{u}^2 + \tilde{v}^2)^{1/2}\tilde{u} + \tilde{\eta}_u, \tag{7}$$

$$\frac{d}{d\tilde{t}}\tilde{v} = -(\tilde{u}^2 + \tilde{v}^2)^{1/2}\tilde{v} + \tilde{\eta}_v, \tag{8}$$

$$\frac{d}{d\tilde{t}}\tilde{\eta}_u = -\frac{1}{\alpha}\tilde{\eta}_u + \frac{\beta}{\alpha}\dot{\tilde{W}}_1, \quad \text{and} \tag{9}$$

$$\frac{d}{d\tilde{t}}\tilde{\eta}_v = -\frac{1}{\alpha}\tilde{\eta}_v + \frac{\beta}{\alpha}\dot{\tilde{W}}_2, \tag{10}$$

depends only on two dimensionless parameters: the relative magnitude of the noise and nonlinear dynamical time scales

$$\alpha = \frac{\tau}{\theta}, \tag{11}$$

and the quantity

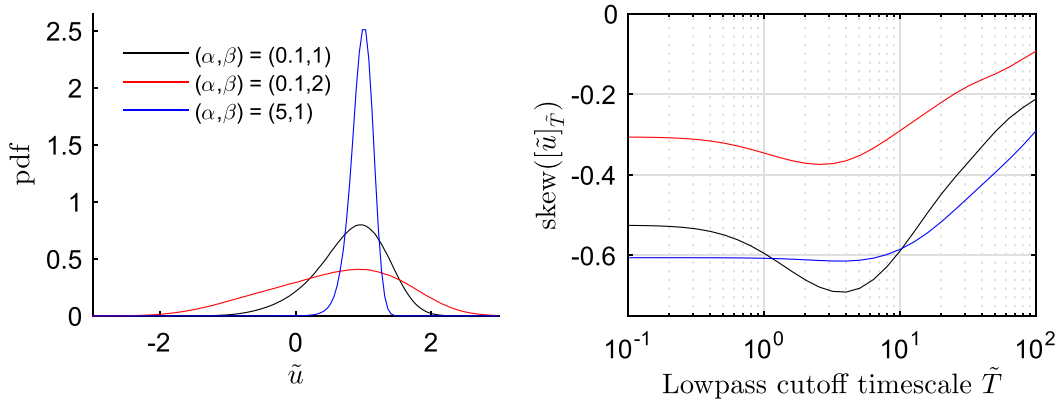

FIG. 5. (left) Pdfs of $\tilde{u}$ from simulations of the nondimensional model Eqs. (7)–(10) for three representative pairs of parameter values. (right) Variations of low-pass-filtered model skewness, skew($[\tilde{u}]_{\tilde{T}}$), as functions of cutoff time scale $\tilde{T}$ for the three representative parameter pairs.

$$\beta = \left(\frac{\sigma^4 c_d}{h \langle \Pi_v \rangle^3} \right)^{1/4}, \tag{12}$$

which scales the size of the fluctuations of $(\tilde{u}, \tilde{v})$ relative to the mean.

To characterize the statistics of $\tilde{u}$ and $[\tilde{u}]_T$ from the model, realizations of 10^6 nondimensional time units were carried out using a forward-Euler approximation to the stochastic differential equations (7)–(10) with time step 4×10^{-3} (Kloeden and Platen 1992). These simulations were obtained for a range of values of the nondimensional parameters α and β.

As discussed in Monahan (2004, 2006a), the distribution of $\tilde{u}$ has by construction a positive mean around which fluctuations are asymmetric with a negative skewness. Examples of simulated pdfs of $\tilde{u}$ for different representative parameter values are presented in the left panel of Fig. 5. In all cases, the mode of the distribution is near $\tilde{u} = 1$. As β increases, the distribution widens and the mean of $\tilde{u}$ decreases (as a result of the characteristic asymmetry of the distribution and the approximately constant value of the mode). A more comprehensive representation of the statistics of $\tilde{u}$ is presented in contour plots of mean($\tilde{u}$), std($\tilde{u}$), and skew($\tilde{u}$) as functions of α and β (Fig. 6). The mean of $\tilde{u}$ is an increasing function of α and a decreasing function of β; the opposite is true of std($\tilde{u}$). For small values of α [approaching the white noise limit considered in Monahan (2006a)], the magnitude of the skewness of $\tilde{u}$ decreases monotonically (fluctuations become more symmetric) as β increases. This gradient is reversed for larger values of α. While the white noise model of Monahan (2006a) generally underestimates the magnitude of the observed along-wind skewness (Thompson et al. 2014), allowing for memory in the ageostrophic driving fluctuations (η_u, η_v) typically increases the magnitude of skew($\tilde{u}$). The largest magnitudes of simulated skewness are found for α of order 1–10 (i.e., when the characteristic time scale τ of the driving noise is about the size of or somewhat larger than the dynamical time scale θ).

The simulated time series show an enhancement of skewness under low-pass filtering that is similar to that of the observations. This fact is illustrated in the right panel Fig. 5 for the three representative pairs of (α, β) values discussed above. The enhancement is most pronounced for the pair $(\alpha, \beta) = (0.1, 1)$, corresponding to a situation of fast (relative to the dynamical time scale) and moderately sized driving fluctuations. For larger values of α and β, the skewness enhancement is reduced. In particular, for $(\alpha, \beta) = (5, 1)$ (corresponding to relatively slow driving fluctuations of moderate size), the enhancement is negligible. In this case, the filtering initially has no effect on skew($[\tilde{u}]_{\tilde{T}}$) as $\tilde{T}$ increases and results in a systematic decrease for $\tilde{T}$ beyond a threshold value of about 5. For the three cases considered, the value of $\tilde{T}$ resulting in the largest absolute skewness is in the range between about 2 and 6.

The effect of filtering on skewness at these representative parameter value pairs is reflected in the general structure of skew($[\tilde{u}]_{\tilde{T}_{\min}}$), skew($[\tilde{u}]_{\tilde{T}_{\min}}$) − skew($\tilde{u}$), and $\tilde{T}_{\min}$ as functions of α and β (Fig. 6). The general features of the skew($[\tilde{u}]_{\tilde{T}}$) surface are similar to those of skew($\tilde{u}$); the difference between the two reveals the enhancement of skewness by filtering. This enhancement is most prominent for $\alpha < 1$ and β small to moderately large, corresponding to driving fluctuations that are fast (relative to the dynamical time scale θ) and of moderate amplitude. The skewness enhancement generally decreases as α and β increase. Consistent with

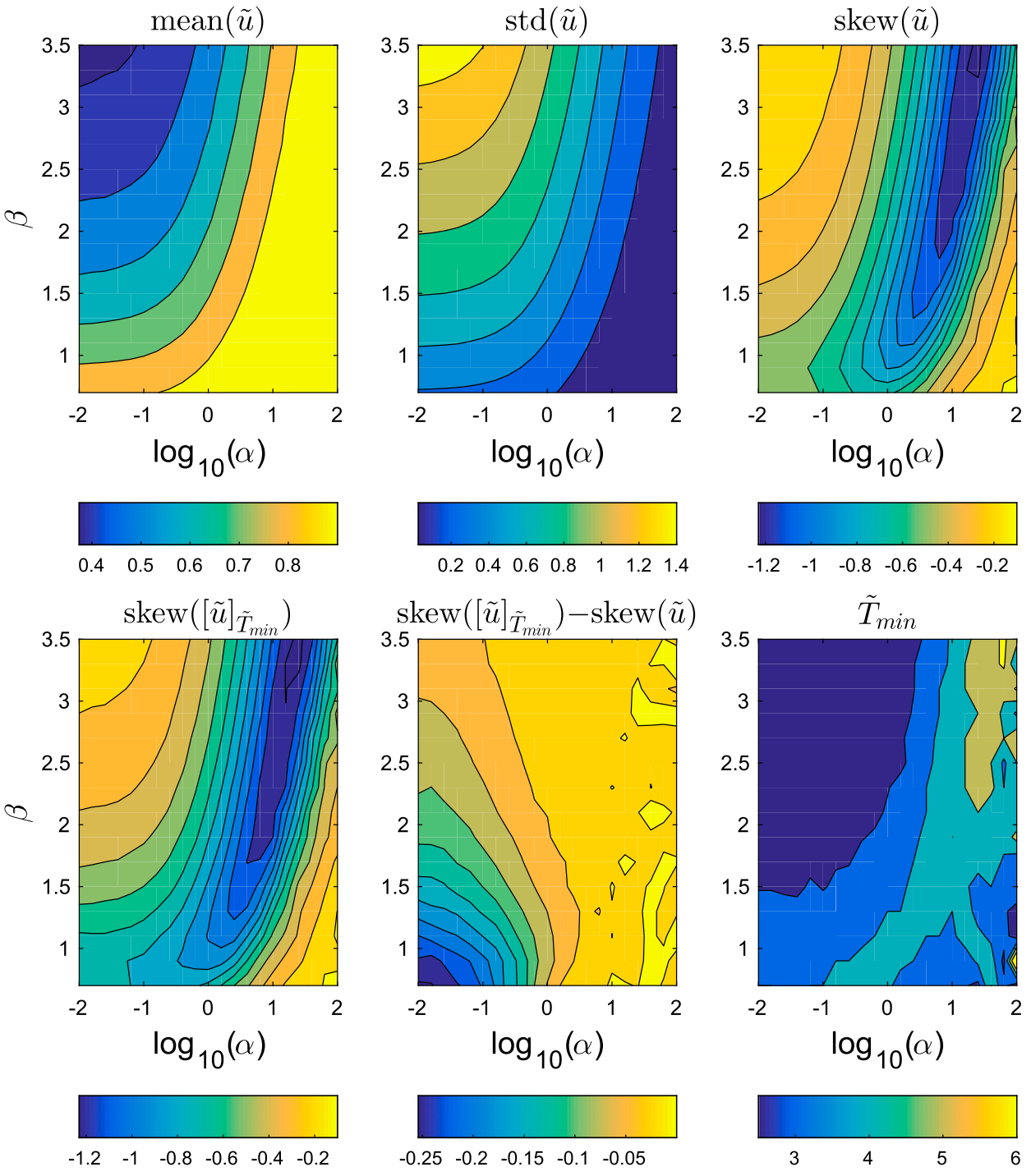

FIG. 6. Simulated statistics of $\tilde{u}$ from the nondimensional model Eqs. (7)–(10) as functions of the model parameters α and β. Shown are (top) the simulated mean, standard deviation, and skewness of unfiltered $\tilde{u}$ and (bottom) the most negative filtered skewness, skew($[\tilde{u}]_{\tilde{T}_{\min}}$), the difference between skew($\tilde{u}$) and skew($[\tilde{u}]_{\tilde{T}_{\min}}$), and value of $\tilde{T}_{\min}$.

examples considered in Fig. 5, values of $\tilde{T}_{\min}$ range between slightly more than 2 to about 6.

By construction in this model, the quadratic nonlinearity in Eqs. (7) and (8) is responsible for the skewness of the simulated along-mean wind component. The skewness enhancements are most pronounced when the time scale of the driving fluctuations is shorter than the nonlinear dynamical time scale

TABLE 1. Hand-tuned model parameter values at the representative locations considered in Fig. 7.

Location	α	β	U (m s^{-1})	θ (h)
1°N, 155°W	0.01	1	4.5	60
27°N, 155°W	5	1	4.5	10
47°N, 155°W	0.1	1	6	30

θ. Furthermore, the value of θ determines the (dimensional) filtering time scale of maximum enhancement $T_{\min}$ (to within a factor of about 2–6). These results indicate that the dynamical nonlinearity time scale is playing a controlling role not only in producing the skewness, but in determining how skewness changes with filtering. The similarity of the dependence of modeled skew($[\tilde{u}]_{\tilde{T}}$) on $\tilde{T}$ (Fig. 5) to that seen in observations (Fig. 2) suggests that the same is true of the observed skewness of sea surface winds. These results are consistent with the hypothesis presented in Proistosescu et al. (2016) that the general decrease of radiosonde temperature skewness with filtering they find is a consequence of the dynamical cause of non-Gaussianity operating on time scales shorter than the decorrelation time.

Estimation of the parameters of a stochastic differential equation such as Eqs. (1)–(4) from observations of u and v but without corresponding observations of η_u and η_v remains a subject of ongoing research (e.g., Chen et al. 2014). In the absence of a systematic procedure to estimate model parameters for all observational locations, ''hand tuned'' estimates were obtained at the representative locations considered in Figs. 1, 2, and 4 (Table 1). These estimates [which were based on the power spectrum and skewness of the observed $\tilde{u}$ and the value of mean(u) at these locations, and a value of $c_d = 1.3 \times 10^{-3}$] were determined by inspection and are not the result of a formal optimization. Nevertheless, the agreement between observed and modeled spectra and skewness values is generally good (Fig. 7). By construction, the model does not reproduce the observed sharp diurnal and semidiurnal peaks of observed u. As well, the model is unable to account for the ENSO-related variability at subannual frequencies observed at 1°N, 155°W. Because about 24% of the variance of u at this location is on frequencies lower than 1/365 cpd, the model fit at this equatorial point is based on the part of the power spectrum with $f > 1/365$ cpd and is scaled by a factor of 0.76 in Fig. 7.

The estimated value of θ for the midlatitude location 47°N, 155°W is 30 h, broadly consistent with the fact that in the midlatitudes values of $T_{\min}$ are on the order of a few to 10 days. Similarly, the subtropical estimate of θ at 27°N, 155°W is about 10 h, consistent with a value of $T \sim$ 1–2 days separating values below which low-pass filtering has little effect on skew($[u]_T$) and above which the skewness magnitude is substantially reduced. It is noteworthy that the values of θ and the filter time scales above which the skewness magnitude systematically decreases with increasing T are smaller in the subtropics than they are in the midlatitudes despite similar ranges of boundary layer depth and surface wind speed scales in these two regions. In the subtropics, the autocorrelation time scales are relatively long (e.g., Monahan 2012), as can also be seen in the location of the peak of the power spectrum (Fig. 7). This fact is consistent with the relatively large value of α estimated for 27°N, 155°W. Furthermore, the $(\alpha, \beta) = (5, 1)$ pdf in Fig. 5 resembles a subtropical along-mean wind component distribution, and the shape of the curve of skew($[\tilde{u}]_{\tilde{T}}$) as a function of $\tilde{T}$ is similar to observed curves in the subtropics such as that at 27°N, 155°W (Fig. 2). It is not clear why the corresponding dimensional time scales θ are smaller than those in the midlatitudes.

It is clear from inspection of Fig. 4 that a substantial contribution to the skewness at 1°N, 155°W comes from low-frequency ENSO-related variability that the model is unable to represent. As such, it is not surprising that while the sign of the modeled skew(u) is correct its magnitude is too small (Fig. 7). Furthermore, the fact that the idealized model is unable to account for the very strong enhancement of skewness and the large values of $T_{\min}$ in the equatorial band (particularly around 150°W) is likely a result of the simple representation of (η_u, η_v) as single-time scale red noise processes, without accounting for the wavelike nature of large-scale equatorial disturbances and the quasi-periodic character of ENSO. Inspection of Fig. 4 also suggests that in the eastern equatorial Pacific region most affected by ENSO, the driving ageostrophic tendency η_u may itself be non-Gaussian. Interestingly, the area around 150°W of largest skewness enhancement is that in which westerly wind bursts are most pronounced (e.g., Tziperman and Yu 2007).

The correlated additive–multiplicative noise process has been proposed as a generic model for non-Gaussian variability of atmosphere and ocean quantities. By definition, the CAM noise process $x(t)$ is described by the stochastic differential equation

$$\frac{dt}{dt} = Ax - \frac{1}{2}Eg + (Ex + g)\dot{W}_1 + b\dot{W}_2, \qquad (13)$$

with A, b, g, and E being constants and W_1 and W_2 being independent white noise processes (e.g., Sardeshmukh

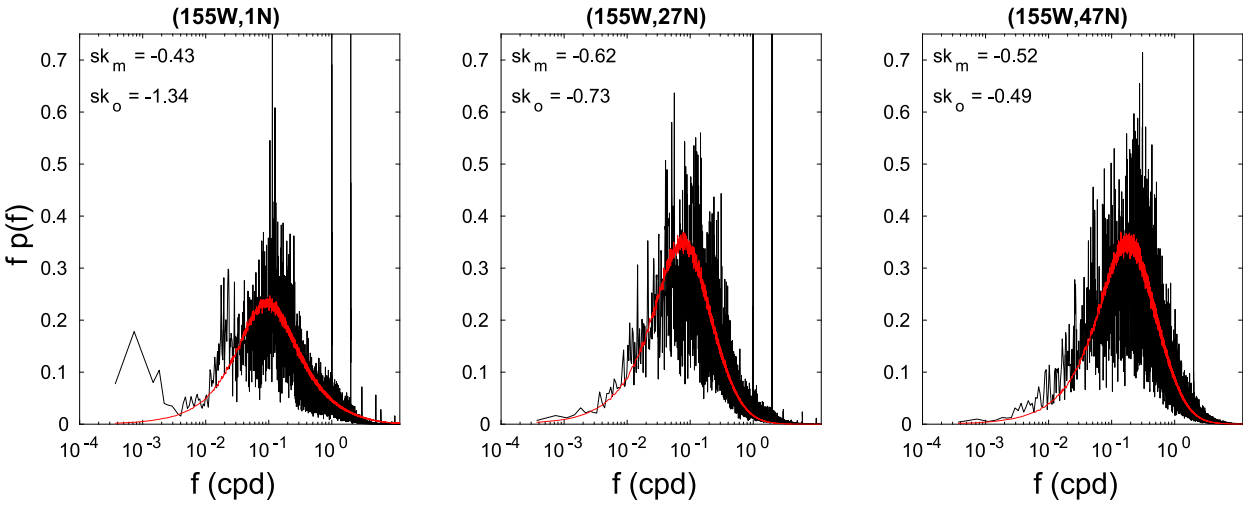

FIG. 7. Observed (black) and modeled (red) power spectra of u at the representative locations from Figs. 1, 2, and 4. Values of observed and modeled skewness (respectively sk_o and sk_m) are given in the upper left of each panel. Model parameters used for the simulations were obtained by hand-tuning the model to the observed mean(u) and the power spectra and skewness values of u. Because the model is unable to account for low-frequency ENSO-related variability, the simulated power spectrum at 1°N, 155°W has been scaled by a factor of 0.76.

and Sura 2009; Penland and Sardeshmukh 2012). Considering a particular CAM process, Proistosescu et al. (2016) found that it does not display the nonmonotonic behavior of the skewness of sea surface winds with filtering. To extend this earlier result, the analysis presented in Fig. 1 is repeated for a range of different CAM processes with different skewness values (obtained by varying the parameter E). Plots of the skewness of bandpass-filtered x for $(A, b, g) = (-1.5, 1, 1)$ and different values of E (corresponding to unfiltered skewness values of 0.34, 0.74, and 1.33) are presented in Fig. 8. It is evident that this process, in which the skewness is associated with fast-time-scale multiplicative noise, cannot represent the enhancement of skewness of u under filtering seen in Fig. 1.

5. Conclusions

The systematic enhancement of skewness of the along-mean wind component of sea surface winds (generally the component with the most pronounced skewness) by low-pass filtering is evident both in observations and in an idealized model of the near-surface momentum budget. Model results indicate that for this field a primary control on the influence of filtering on non-Gaussianity is the ratio of the characteristic time

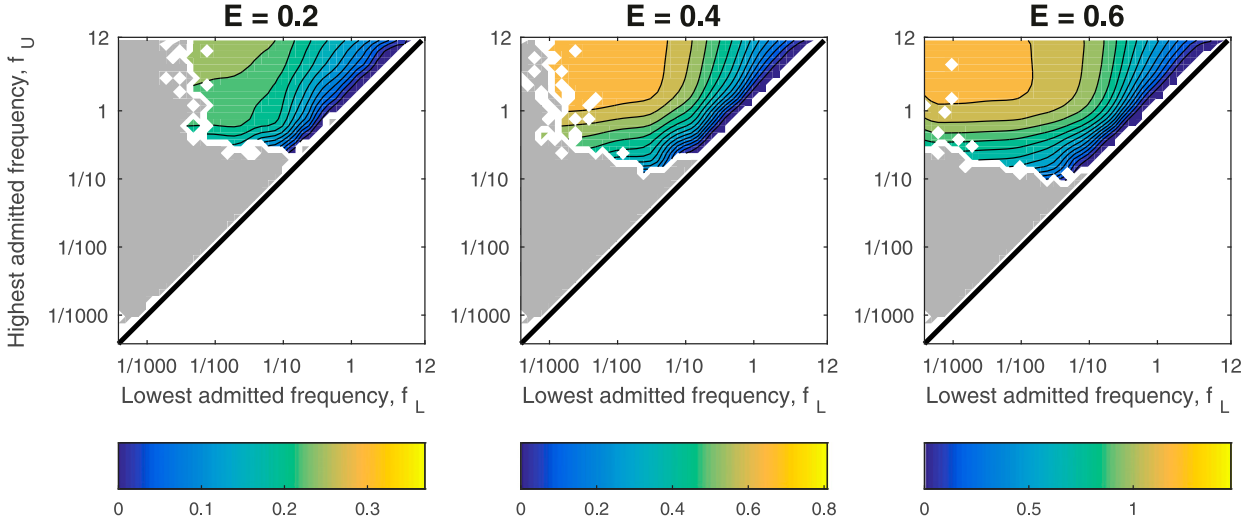

FIG. 8. As in Fig. 1, but for CAM processes with $(A, b, g) = (-1.5, 1, 1)$ and $E = 0.2$, 0.4, and 0.6.

scale of the driving fluctuations to the time scale characteristic of the nonlinear dynamics. The results suggest the following interpretation. When the driving fluctuations are fast relative to the nonlinear dynamical time scale, variations of the time series will consist of many fast ''kicks'' on top of a slow, integrated, dynamical response that is responsible for the non-Gaussian structure. By filtering out time scales longer than that of the noise but shorter than the nonlinear dynamics, the rapid fluctuations associated with these kicks are suppressed and the non-Gaussian variability is enhanced (in relative terms). As the filtering time scale becomes large compared to the dynamical time scale, the averaging inherent in low-pass filtering results in a reduction of skewness. When the time scales of the driving noise are long compared to the dynamical time scale, the kicks on time scales shorter than the dynamical time scale are relatively weak and the skewness of the response is unaffected by filtering until the filter time scale exceeds the dynamical time scale.

Rough parameter estimates for idealized model indicate that the nonlinear dynamical time scale in most locations should be on the order of about half a day to a few days, broadly consistent with the response of skewness to low-pass filtering outside of the equatorial band. The enhancement of skewness by filtering is most pronounced in the equatorial band, particularly in a region centered around 150°W. The filter time scales of maximum skewness enhancement in these regions are also relatively long, on the subseasonal to seasonal scale. Variability in these regions is dominated by equatorial waves and ENSO, with time scales longer than dominant processes outside the equatorial band. Furthermore, inspection of filtered time series in the region most affected by ENSO suggests that the driving noise processes themselves are non-Gaussian; the simple red-noise model for (η_u, η_v) used in this study is too simple to capture this behavior. It remains unclear why the observed subtropical dynamical time scale of about a day should be smaller than that of the midlatitudes. A more thorough comparison of the model and observations would require estimates of model parameters and of the noise time series (η_u, η_v), which remains a challenge (Thompson et al. 2014; Chen et al. 2014).

The 10-m wind time series considered in this analysis are not observational data, but rather reanalysis model products. Previous comparisons of the representation of the statistics of sea surface winds in earlier generations of reanalyses and remotely sensed observational data indicate that while there may be differences in detail between observations and different reanalyses, the main qualitative features are robust (Monahan 2006b). The MERRA-2 reanalysis product was chosen for the present analysis because of its relatively high resolution in time, allowing for the investigation of subdaily variability. A similar analysis using 6-hourly 10-m wind from the European Centre for Medium-Range Weather Forecasts (ECMWF) interim reanalysis (ERA-Interim) product (Dee et al. 2011) produced results similar to those presented here (not shown). Note that a detailed analysis of the MERRA-2 representation of the atmospheric structure during large El Niño events shows that the reanalysis product is in excellent agreement with observations (Lim et al. 2017).

Standardizing the wind components by estimates of the seasonal cycles of the mean and standard deviation reduces the seasonal nonstationarity but does not eliminate it. An interesting direction of future study would be to analyze the behavior of the skewness of the along-mean wind component under filtering using output from an atmospheric circulation model with no seasonal variations. Because of the simplicity of the physical mechanism primarily responsible for the non-Gaussianity of surface wind components captured in Eqs. (1)–(4), this behavior in such modeled winds should be similar to that of observations—with the possible exception of the equatorial Pacific ocean, in which suppression of the seasonal cycle may affect ENSO dynamics.

Proistosescu et al. (2016) emphasized the utility of the bispectrum as a tool to investigate the role of interactions between frequencies in the production of skewness. An interesting direction of future study will be to use the bispectrum to investigate these interactions in both the reanalysis winds and the idealized model. Such an analysis would provide valuable new insight into the physical mechanisms responsible for observed deviations from Gaussianity in near-surface winds.

While this study has focused on the effects of filtering on the skewness of sea surface winds, there will be corresponding effects on other aspects of the distribution such as kurtosis. Proistosescu et al. (2016) showed that the kurtosis of air temperature is modified by filtering in a manner that is distinct from that of the skewness. A consideration of the effects of filtering on the kurtosis (and other measures of non-Gaussianity) of sea surface winds is another interesting direction of future study.

Finally, the results of the present study also suggest an approach to investigating the relative importance of dynamical nonlinearities and multiplicative noise in producing non-Gaussian variability of atmospheric or oceanic fields. While CAM noise is able to account for many aspects of observed deviations from Gaussianity (e.g., Sura 2011; Sura and Hannachi 2015), it does not reproduce the observed skewness enhancement by filtering in sea surface winds. The analysis presented in this study indicates an essential role for dynamical nonlinearities in the generation of skewness in this field

and its enhancement by filtering. The observable considered in this study provides one specific test allowing distinctions to be made between situations in which observed non-Gaussianity can be accounted for by multiplicative noise, and when dynamical nonlinearities must be invoked. Interesting directions of future study are the application of such tests to other fields, using this or other novel observables.

Acknowledgments. I gratefully acknowledge support from the Natural Sciences and Engineering Research Council of Canada (NSERC; Grant RGPIN-2014-06509). I would also like to thank Carsten Abraham, Christian Proistosescu, Tim DelSole, and one anonymous reviewer for their helpful comments on the manuscript. This research was carried out when I was a visitor at the Statistical and Applied Mathematical Sciences Institute (SAMSI), whose hospitality I gratefully acknowledge. Data were obtained from the Global Modeling and Assimilation Office (GMAO 2015; https://doi.org/10.5067/3Z173KIE2TPD).

REFERENCES

Chen, N., D. Giannakis, R. Herbei, and A. J. Majda, 2014: An MCMC algorithm for parameter estimation in signals with hidden intermittent instability. *SIAM/ASA J. Uncertainty Quantif.*, **2**, 647–669, https://doi.org/10.1137/130944977.

Dee, D. P., and Coauthors, 2011: The ERA-Interim reanalysis: Configuration and performance of the data assimilation system. *Quart. J. Roy. Meteor. Soc.*, **137**, 553–597, https://doi.org/10.1002/qj.828.

Gelaro, R., and Coauthors, 2017: The Modern-Era Retrospective Analysis for Research and Applications, version 2 (MERRA-2). *J. Climate*, **30**, 5419–5454, https://doi.org/10.1175/JCLI-D-16-0758.1.

GMAO, 2015: MERRA-2 inst1_2d_atm_Nx: 2d, 1-hourly, instantaneous, single-level, assimilation, single-level diagnostics V5.12.4, Goddard Space Flight Center Distributed Active Archive Center (GSFC DAAC), accessed July–August 2017, https://doi.org/10.5067/3Z173KIE2TPD.

Kloeden, P. E., and E. Platen, 1992: *Numerical Solution of Stochastic Differential Equations*. Springer-Verlag, 636 pp.

Lim, Y.-K., R. M. Kovach, S. Pawson, and G. Vernieres, 2017: The 2015/16 El Niño event in context of the MERRA-2 reanalysis: A comparison of the tropical Pacific with 1982/83 and 1997/98. *J. Climate*, **30**, 4819–4842, https://doi.org/10.1175/JCLI-D-16-0800.1.

Monahan, A. H., 2004: A simple model for the skewness of global sea surface winds. *J. Atmos. Sci.*, **61**, 2037–2049, https://doi.org/10.1175/1520-0469(2004)061<2037:ASMFTS>2.0.CO;2.

——, 2006a: The probability distribution of sea surface wind speeds. Part I: Theory and SeaWinds observations. *J. Climate*, **19**, 497–520, https://doi.org/10.1175/JCLI3640.1.

——, 2006b: The probability distribution of sea surface wind speeds. Part II: Dataset intercomparison and seasonal variability. *J. Climate*, **19**, 521–534, https://doi.org/10.1175/JCLI3641.1.

——, 2012: The temporal autocorrelation structure of sea surface winds. *J. Climate*, **25**, 6684–6700, https://doi.org/10.1175/JCLI-D-11-00698.1.

Penland, C., and P. D. Sardeshmukh, 2012: Alternative interpretations of power-law distributions found in nature. *Chaos*, **22**, 023119, https://doi.org/10.1063/1.4706504.

Proistosescu, C., A. Rhines, and P. Huybers, 2016: Identification and interpretation of nonnormality in atmospheric time series. *Geophys. Res. Lett.*, **43**, 5425–5434, https://doi.org/10.1002/2016GL068880.

Sardeshmukh, P. D., and P. Sura, 2009: Reconciling non-Gaussian climate statistics with linear dynamics. *J. Climate*, **22**, 1193–1207, https://doi.org/10.1175/2008JCLI2358.1.

——, G. P. Compo, and C. Penland, 2015: Need for caution in interpreting extreme weather statistics. *J. Climate*, **28**, 9166–9187, https://doi.org/10.1175/JCLI-D-15-0020.1.

Schneider, T., T. Bischoff, and H. Płotka, 2015: Physics of changes in synoptic midlatitude temperature variability. *J. Climate*, **28**, 2312–2331, https://doi.org/10.1175/JCLI-D-14-00632.1.

Sura, P., 2011: A general perspective of extreme events in weather and climate. *Atmos. Res.*, **101**, 1–21, https://doi.org/10.1016/j.atmosres.2011.01.012.

——, and A. Hannachi, 2015: Perspectives of non-Gaussianity in atmospheric synoptic and low-frequency variability. *J. Climate*, **28**, 5091–5114, https://doi.org/10.1175/JCLI-D-14-00572.1.

Teng, Q., A. H. Monahan, and J. C. Fyfe, 2004: Effects of time averaging on climate regimes. *Geophys. Res. Lett.*, **31**, L22203, https://doi.org/10.1029/2004GL020840.

Thompson, W. F., A. H. Monahan, and D. Crommelin, 2014: Parametric estimation of the stochastic dynamics of sea surface winds. *J. Atmos. Sci.*, **71**, 3465–3483, https://doi.org/10.1175/JAS-D-13-0260.1.

Tziperman, E., and L. Yu, 2007: Quantifying the dependence of westerly wind bursts on the large-scale tropical Pacific SST. *J. Climate*, **20**, 2760–2768, https://doi.org/10.1175/JCLI4138a.1.